Ultrasonics Sonochemistry 103 (2024) 106774

Contents lists available at ScienceDirect

Ultrasonics Sonochemistry

journal homepage: www.elsevier.com/locate/ultson

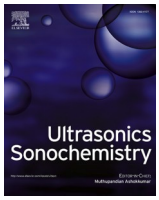

Ultrasonic aerosol agglomeration: Manipulation of particle deposition and its impact on air filter pressure drop

Pengzhan Liu [a,b,1], Xin Zhang [a,1], Guicai Liu [c], Shi Hao Lim [a], Man Pun Wan [b], Grzegorz Lisak [c,d], Bing Feng Ng [b,*]

[a] Energy Research Institute @ NTU, Nanyang Technological University, Singapore 639141, Singapore
[b] School of Mechanical and Aerospace Engineering, Nanyang Technological University, Singapore 639798, Singapore
[c] Residues and Resource Reclamation Centre, Nanyang Environment and Water Research Institute, Nanyang Technological University, Singapore 637141, Singapore
[d] School of Civil and Environmental Engineering, Nanyang Technological University, Singapore 639798, Singapore

ARTICLE INFO

Keywords:
Ultrasound
Manipulation
Agglomeration
Aerosol
Filtration
Pressure drop

ABSTRACT

Acoustic agglomeration is a technique that leverages on sound waves to promote the collision of aerosol particulate matter, thus leading to the formation of larger particle agglomerates. In this study, this acoustics-driven phenomenon is demonstrated for its usefulness as an aerosol pre-conditioning method to significantly enhance the efficiency of filtration systems in particle treatment processes. Specifically, favorable changes in pressure drop across the filters are observed as a result of receiving less particle mass, for which filters are shown to be able to have their operational life extended remarkably by more than 50%. The involved ultrasonic aerosol agglomeration mechanisms are unveiled through numerical simulations, and the effects of residence time, sound pressure level, and initial particle number concentration on agglomeration performances are experimentally investigated. In addition, validations and measurements of filter pressure drop are obtained through a series of experiments. This study provides a comprehensive overview to the design and performance characterization of acoustics-agglomeration-enhanced filtration systems, which could potentially derive energy savings for fan power in ventilation systems and be scaled up for applications in industrial plants for reducing carbon emissions.

1. Introduction

The ability to effectively manipulate and process aerosol particles has been gaining increasing attention in light of the global quests for carbon neutrality, energy saving, and emission reduction [1–5]. It has been proven that both chemical [6–8] and physical methods [9–14] can offer effective manipulation/treatment of aerosol particles. In the latter, the physical methods include the use of turbulence/vortex [9,11,15], magnetics [12,16], electrics [14,17,18], and acoustics [1,19–26] for aerosol particle manipulation. Among them, the acoustic manipulation method, specifically acoustic agglomeration (AA), harnesses sound waves to cause additional motions and collisions of aerosol particles to achieve particle coagulation [1]. Different from the acoustic mechanisms utilized for particle manipulation in fluidic environments such as acoustic radiation forces and acoustic streaming [27–29], physical mechanisms involved in acoustic aerosol agglomeration include the orthokinetic and hydrodynamic effects [30,31]. Through the combined orthokinetic and hydrodynamic effects, smaller aerosol particles cluster to form larger particles that result in changes to airborne particle size distribution (PSD) and concentration levels. Compared with other physical aerosol manipulation mechanisms, AA can circumvent the use of large-scale electric or magnetic systems, as well as complex flow regulators in aerosol chambers or tunnels.

Throughout the years, many researchers have demonstrated the effectiveness of AA for controlling aerosol emission [1,32–37], in which audible speakers are mostly adopted as sound sources. For instance, Yang *et al.* recently have applied AA to treat oil particles with a sound pressure level (SPL) higher than 130 dB and a frequency between 1000 Hz and 5000 Hz [38]. However, audible sound with high SPLs may cause serious noise issues and damage to human hearing especially when there are operators around AA processes. Therefore, the use of airborne ultrasound for further development of AA has been highlighted [30], and some researchers have successfully established and deployed efficient ultrasonic systems to substitute audible speakers for AA of aerosol

* Corresponding author.
E-mail address: bingfeng@ntu.edu.sg (B. Feng Ng).
[1] These two authors contributed equally.

https://doi.org/10.1016/j.ultsonch.2024.106774
Received 6 December 2023; Received in revised form 12 January 2024; Accepted 17 January 2024
Available online 20 January 2024

particles [21,39,40].

Although the ability of AA to manipulate airborne PSD and concentration levels has been proven through numerous experimental studies [1,30], its direct usefulness and application in pollution control is still lacking. A potential use for AA is in filtration systems where the pre-treatment of aerosols upstream of air filters could enhance particle removal efficiency. The rationale is that smaller particles agglomerate under sonication to form larger particles that can be more easily captured by the filters [38,41,42]. However, this increase in particle removal efficiency is often accompanied by faster increase in filter pressure drop (PD), thus requiring more energy to be consumed by the exhaust fans (to overcome filter PD). This trade-off remains a challenge to be resolved before AA can be efficiently applied to pollution control systems involving filtration processes.

In this study, we address this challenge by demonstrating the increase of aerosol filtration efficiency without significant increase in PD of air filters in a purpose-built aerosol wind tunnel system. This is achieved by combining AA with a mechanical particle separation process. Specifically, aerosol particles first undergo AA to form larger particle agglomerates and then undergo deposition in a particle separation component. Owing to the reduction in particle mass through the combined action of these two processes, the downstream air filter receives less particle mass and thus experiences lower PD compared with the scenario where there is no AA process. Additionally, an airborne ultrasonic system is used to perform AA to avoid the issue related to audible noise caused in human working environment, bringing this study closer to its practical implementation. In the following sections, we will discuss the mechanisms of ultrasonic aerosol agglomeration, and further demonstrate its usefulness as a particle pre-conditioning method to reduce the filtration burden on air filters when coupled with a prior particle separation process. Different parameters affecting the performances of ultrasonic aerosol agglomeration will also be discussed.

2. Experimental setup

The experimental setup of an aerosol wind tunnel for ultrasonic aerosol agglomeration in this study is shown in Fig. 1. The aerosol wind tunnel is composed of multiple modular sections that include an inlet, a dust diffusing chamber, an ultrasonic agglomeration zone, a particle separation device, a filter test section, a fan, and an outlet. The inlet section contains an entrance to ambient air which is cleaned by a High-Efficiency Particulate Air (HEPA) filter. In addition, the inlet section contains a bypass which allows particles that are aerosolized by a dust generator (SAG 410/H, TOPAS Inc.) to be dispensed into the tunnel. For each run of experiments, new standard Arizona A4 test dust (PTI Inc.) is used. Downstream of the inlet section, a lobe mixer allows particles to be uniformly mixed with the ambient air in the diffuser.

Following which, the particles enter the ultrasonic agglomeration zone which has a total length of 3 m and a diameter of 200 mm. A customized ultrasonic transducer with a working frequency of 21 kHz (Pusonics Inc.), of which the main body is made by titanium, is excited by a matched power supply to provide an ultrasonic field within the

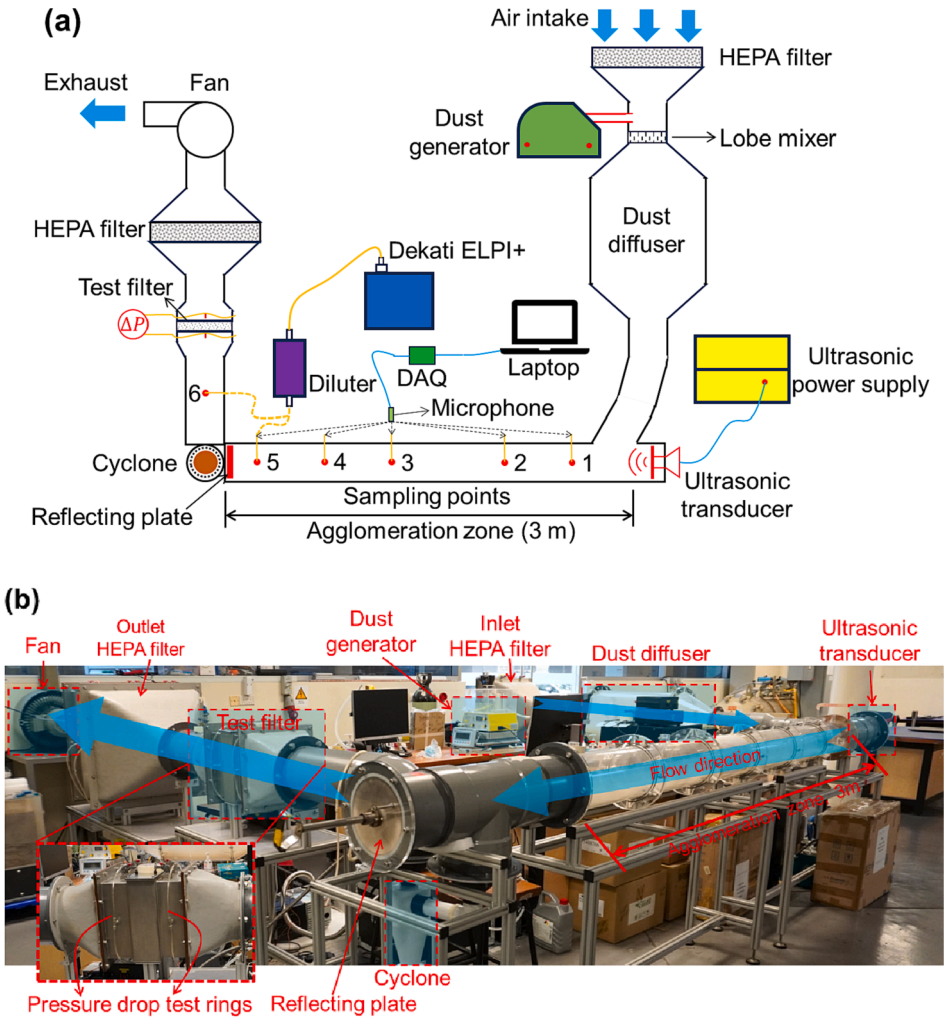

Fig. 1. Aerosol wind tunnel-based experimental setup. (a) Schematic. (b) Photo.

agglomeration zone. Five sampling points are distributed along the agglomeration zone to allow for measurement of local SPLs using a microphone (Brüel & Kjær Type 4954) that is connected to a laptop through a data acquisition (DAQ) card. The sampling points are also used to measure particle number concentrations (PNCs) using a particle size spectrometer (ELPI+, Dekati Inc.) with a diluter. In addition, flow speeds in the agglomeration zone are measured by a hot-wire anemometer (Center 332) through these sampling points.

As shown in Fig. 1, a reflecting plate is positioned at the end of the agglomeration zone for the formation of a standing wave ultrasonic field. It is anticipated that a standing wave ultrasonic field enables better agglomeration performance as compared to its corresponding traveling wave ultrasonic field when the sound parameters are kept the same [30]. A particle separation device is arranged behind the agglomeration zone to capture the larger particle agglomerates that are formed through the ultrasonic agglomeration process. Without this particle separation device, the downstream air filter with pre-ultrasonicated aerosol particles would receive particle mass that is almost the same as the condition without ultrasonication of aerosol particles, leading to insignificant changes in PD across the filters. Consequently, the incorporation of such a particle separation device after the ultrasonic agglomeration process becomes essential to achieving the concurrent improvement in filtration efficiency with desired changes to filter PD. Here, a cyclone separator (HG0011718, OEM) is used as the particle separation device, and other types such as settling chambers/pipes can also be considered [42].

After the cyclone separator, another sampling point is positioned before test filters to measure and compare PNCs downstream of the cyclone separator. For the filter PD tests, M6 (BS EN 779) filters (Camfil Inc.) are used, and a custom-made digital manometer (Bluewind Inc.) is installed to measure PD across filters using the connected test rings shown in Fig. 1(b). For each PD test, a new M6 filter is used throughout the entire experimental process. In the outlet section, another HEPA filter is installed to clean the air before it is released into an outdoor environment. The exhaust fan (TECO ELECTRIC & MACHINERY PTE LTD) controls the flow speed within the aerosol wind tunnel through a combination of the power setting and the throttling valve.

3. Numerical setup

3.1. Modelling of ultrasonic agglomeration zone

A model of the agglomeration zone with the corresponding boundary conditions is generated for numerical simulations of the vibration field in the ultrasonic transducer and the resultant ultrasonic field in the agglomeration zone (Fig. 2(a)). Simulations are performed by the commercial software COMSOL Multiphysics 6.1 (Burlington, MA, USA) based on the finite element method (FEM). Herein, given the limited computation resources available, a simplified two-dimensional (2D) model is used. As shown in Fig. 2(a), multiple hard walls are used to mimic the internal walls of the tunnel and the reflecting plate. Two perfectly matched boundaries (PMBs) are imposed to mimic the connecting ports with other modular sections. The vibration excitation (indicated in the dashed red box in Fig. 2(a)) is exerted on the upper part of the transducer in the *x*-direction, and the radiation plate-air interfaces are set as the acoustic-structure boundaries. The acoustic-solid interaction module in COMSOL is employed to implement frequency-domain simulations, and the governing equation for computing the vibration field in the ultrasonic transducer is

$$-\rho_s\omega^2\boldsymbol{u} = \nabla\cdot\mathrm{S} + \boldsymbol{F}_\mathrm{V}\mathrm{e}^{\mathrm{i}\varphi} \tag{1}$$

where ρ_s is the density of solid, ω is the angular frequency, $\boldsymbol{u}$ is the displacement vector, $\boldsymbol{S}$ is the second Piola-Kirchhoff stress, $\boldsymbol{F}_\mathrm{V}$ is the volume force vector, i is the imaginary unit, and φ is the phase angle. The governing equation for computing the ultrasonic field in the agglomeration zone is the lossy Helmholtz equation considering the thermally conducting and viscous effects for sound attenuation [29], which is expressed as

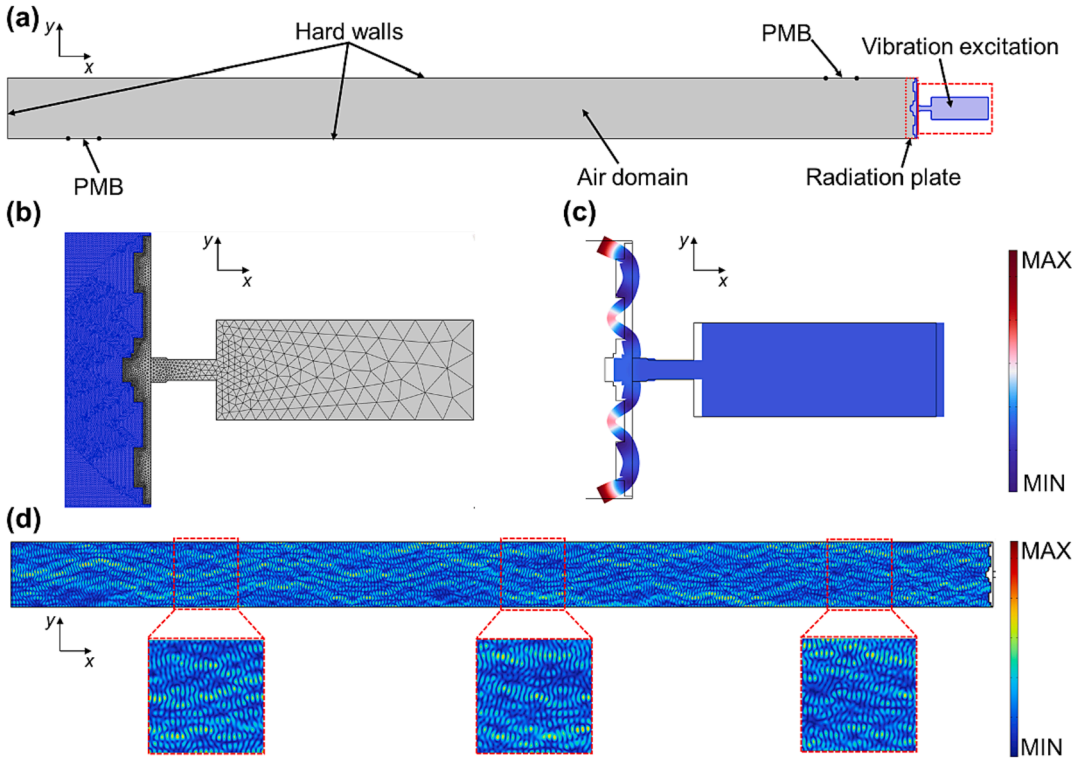

Fig. 2. (a) Physical model and boundary conditions for simulating vibro-acoustic fields. (b) Meshed model around the acoustic-structure boundaries. (c) Simulated vibration mode of the ultrasonic transducer at 21 kHz. (d) Simulated ultrasonic field (absolute acoustic pressure) in the agglomeration zone at 21 kHz.

$$\nabla^2 p + \frac{\omega^2}{c_g^2 + i\frac{\omega}{\rho_g}\left[\frac{4}{3}\mu + \mu_B + \frac{(\gamma-1)k}{C_p}\right]} p = 0 \quad (2)$$

where p is the acoustic pressure and c_g, ρ_g, μ, μ_B, C_p, γ, and k are the sound speed, density, dynamic viscosity, bulk viscosity, heat capacity at constant pressure, ratio of specific heats, and thermal conductivity of gas, respectively. The material parameters used in the simulations are listed in Table 1.

The meshed model around the radiation plate-air interfaces is shown in Fig. 2(b), in which the free triangular mesh is used. To ensure the reliability of simulation results, a maximum element size of 32.4 mm is set in the transducer domain and 1 mm in the air domain (about 6.12 % of the wavelength of the ultrasonic field at 21 kHz).

The simulated vibration mode of the ultrasonic transducer at 21 kHz is shown in Fig. 2(c). It can be observed that the *x*-directional vibration of the transducer's upper part (indicated in the dashed red box in Fig. 2(a)) induces the flexural vibration of the radiation plate through the connecting rod, which provides airborne ultrasound to the agglomeration zone for aerosol agglomeration.

Fig. 2(d) shows the simulated distribution of absolute acoustic pressure in the agglomeration zone at 21 kHz. From the three insets, it can be observed that the standing wave ultrasonic field is well distributed throughout the entire agglomeration zone. Even though the attenuation effects are considered in the simulation of ultrasonic field (Eq. (2)), their effects appear to be insignificant along the agglomeration zone (by comparing the intensities of absolute acoustic pressure at multiple acoustic anti-nodes). This indicates that the airborne ultrasound emitted by this transducer under 21 kHz experiences little attenuation along the length direction of our ultrasonic agglomeration zone.

3.2. Modelling of ultrasonic aerosol agglomeration

The ultrasonic aerosol agglomeration process is modelled to investigate changes in PSD with and without ultrasonication. Here, the PSD function $n(v,t)$ is considered to be only dependent on the time t and the particle volume v. As a result, the agglomeration process is governed by the temporal aerosol evolution equation as [43]

$$\frac{\partial n(v,t)}{\partial t} = \frac{1}{2}\int_0^v \beta(\tilde{v}, v-\tilde{v}) n(\tilde{v},t) n(v-\tilde{v},t) d\tilde{v} - \int_0^\infty \beta(v,\tilde{v}) n(\tilde{v},t) n(v,t) d\tilde{v} \quad (3)$$

where β is the total ultrasonic agglomeration kernel. Typically, there are two types of kernels to be considered in AA; the first one is the orthokinetic kernel [31,44,45], which is expressed as

$$\beta^{OR}(d_1, d_2) = \frac{1}{2}(d_1 + d_2)^2 U_g \eta_{12} \quad (4)$$

Table 1
Material parameters used in the FEM simulations.

Symbol	Quantity	Value for titanium	Value for air
c_g	Sound speed	/	343 m/s
ρ_s/ρ_g	Density	4506 kg/m^3	1.2 kg/m^3
μ	Dynamic viscosity	/	1.82×10^{-5} Pa•s
μ_B	Bulk viscosity	/	5.45×10^{-6} Pa•s
C_p	Heat capacity at constant pressure	/	1015 J/(kg•K)
γ	Ratio of specific heats	/	1.4
k	Thermal conductivity	/	0.026 W/(m•K)
ν	Poisson ratio	0.321	/
E	Young modulus	115.7 GPa	/

where d_1 and d_2 are the particle diameters, U_g is the acoustic velocity of air, and η_{12} is the real part of the entrainment factor difference $H_{12} = H_1 - H_2$. The entrainment factor H is defined as

$$H = \frac{1}{1 - i\omega\tau_d} \quad (5)$$

where τ_d is the dynamic relaxation time of particle and is defined as

$$\tau_d = \frac{\rho_p d_p^2}{18\mu} \quad (6)$$

where ρ_p and d_p are the density (assumed as 1 g/cm^3 here) and diameter of particle, respectively. The other kernel usually considered is the mutual radiation pressure (MRP) kernel that captures the hydrodynamic effect, and is expressed as

$$\beta^{MRP}(d_1, d_2) = \frac{\sqrt{3}\rho_g U_g^2}{144\pi\mu} \frac{d_1^2 d_2^2}{d_1 + d_2} g_{12} \quad (7)$$

where g_{12} is the hydrodynamic interaction function [22]. The total kernel used for the ultrasonic aerosol agglomeration simulations is the sum of the orthokinetic and MRP kernels, which is given as

$$\beta^{total} = \beta^{OR} + \beta^{MRP} \quad (8)$$

As the equation for describing the temporal evolution of PSD (Eq. (3)) is a partial, non-linear, and integro-differential equation, only a limited number of analytical solutions are available. Commonly, numerical methods are employed [22,31,45–48], and here we adopt the sectional method to resolve the PSD under ultrasonic agglomeration [31,47–49]. The detailed implementation strategy of this method is described in our previous study [31].

4. Results and discussions

In a typical experiment, we first set the flow speed inside the agglomeration zone (Fig. 1) as 0.72 m/s, and this gives the residence time of aerosol in the agglomeration zone to be 4.2 s. The ultrasonic transducer is operated under 40 W to avoid rapid heating under its maximum driving power of 50 W. At each sampling point, 20 measurement points of SPL are captured by moving the microphone probe at the same interval along the sectional radial direction. For instance, at sampling point 1 (Fig. 1(a)), the arithmetic mean of 20 values of SPL is obtained to represent the characteristic SPL for this sampling point. The process is then repeated for the other 4 sampling points and their average is used to represent the characteristic SPL for each experimental condition. Following the steps described above, under the transducer driving power of 40 W, the characteristic SPL is obtained to be 137 dB. The dispensing rate of the dust generator is set to be 10 % of the maximum dispensing rate on its front panel, and under the combination of this setting and the flow speed of 0.72 m/s, the initial total PNC generated is denoted as C1 (Table 2).

Fig. 3(a) shows the comparison of the PSD without and with ultrasonication (residence time: 4.2 s; initial total PNC: C1; SPL: 137 dB). Both experimental and simulated results show that with ultrasonication,

Table 2
Experimental parameters for the definition of initial total particle number concentrations (PNCs).

Initial total PNC	Dispensing rate (%)	Flow speed in the agglomeration zone (m/s)
C1	10	0.72
C2-1	15	0.36
C2-2	30	0.72
C2-3	70	1
C3	100	0.72

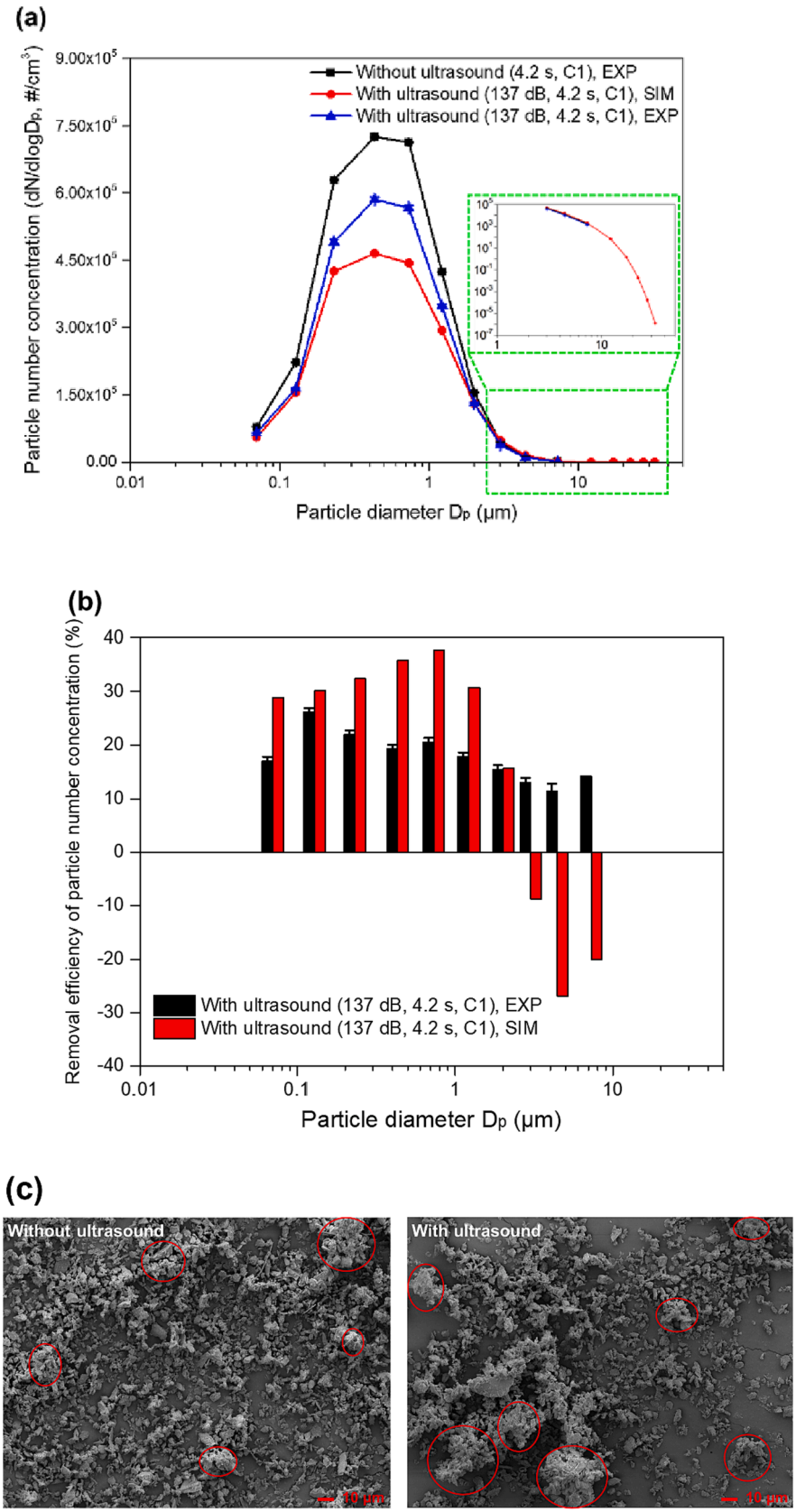

Fig. 3. Comparison of particle and filter characteristics without and with ultrasonication of 137 dB under the residence time of 4.2 s. The initial total particle number concentration is denoted as C1. (a) Particle size distribution. EXP represents the experimental result, and SIM represents the simulated result. (b) Removal efficiency of particle number concentration versus particle diameter. (c) SEM images of particles that are deposited at the bottom of the cyclone. (d) Measured particle size distribution after the cyclone. (e) Measured time-domain pressure drop increment of air filters.

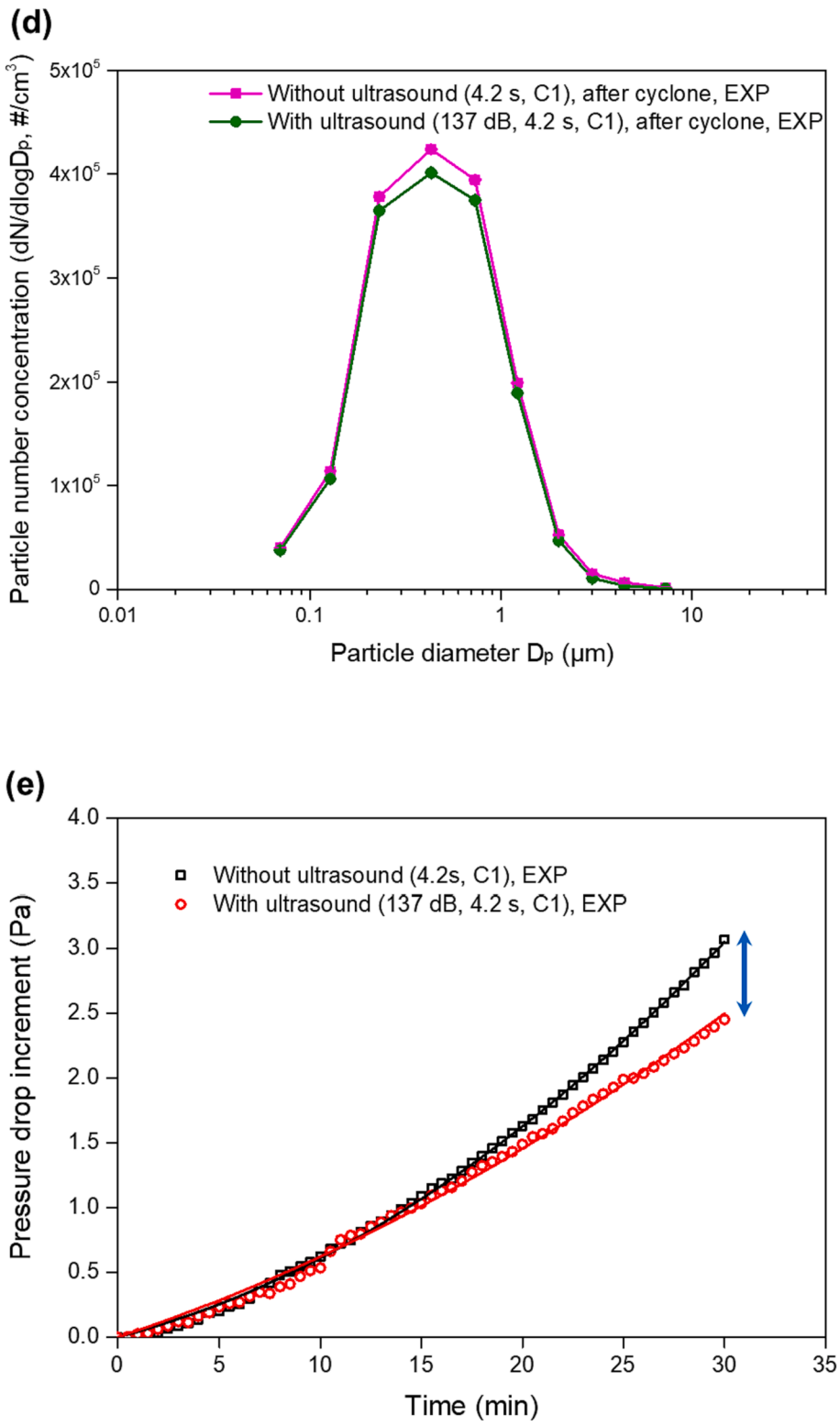

Fig. 3. (*continued*).

the PNCs experience significant drop across the measurable particle size range, especially in the central size range. This indicates that aerosol particles are agglomerated by airborne ultrasound and thus their respective concentrations are decreased accordingly. The difference between the experimental and simulated results may be due to the uneven distribution of SPLs in the experimental tunnel setup as opposed to a constant SPL used in the simulations, which could overpredict the actual ultrasonic aerosol agglomeration performances. Moreover, as the measurable size range of the particle counter is limited to 6 nm to 10 μm, aerosol particles that are larger than 10 μm can only be captured through the simulations, as shown in the inset of Fig. 3(a).

The removal efficiency of PNC at each particle size bin is defined as $(1\text{-}N/N_0) \times 100$ %, where N_0 and N are the PNCs without and with ultrasonication at each particle size bin, respectively. The experimental

and simulated results of removal efficiency of PNC versus particle diameter is shown in Fig. 3(b), where it can be observed that removal efficiencies of PNC are positive across all the particle size bins from 0.1 to 10 μm in the experiments. On the other hand, there is increase in PNCs for the particle size bins from 3 to 10 μm in the simulations due to the agglomeration of smaller particles and the formation of larger particle agglomerates. With higher concentrations of larger particles after ultrasonic agglomeration, it is postulated that the cyclone separator can become more effective in reducing PNC prior to the downstream air filter. As a result, the filter would receive less particle mass and

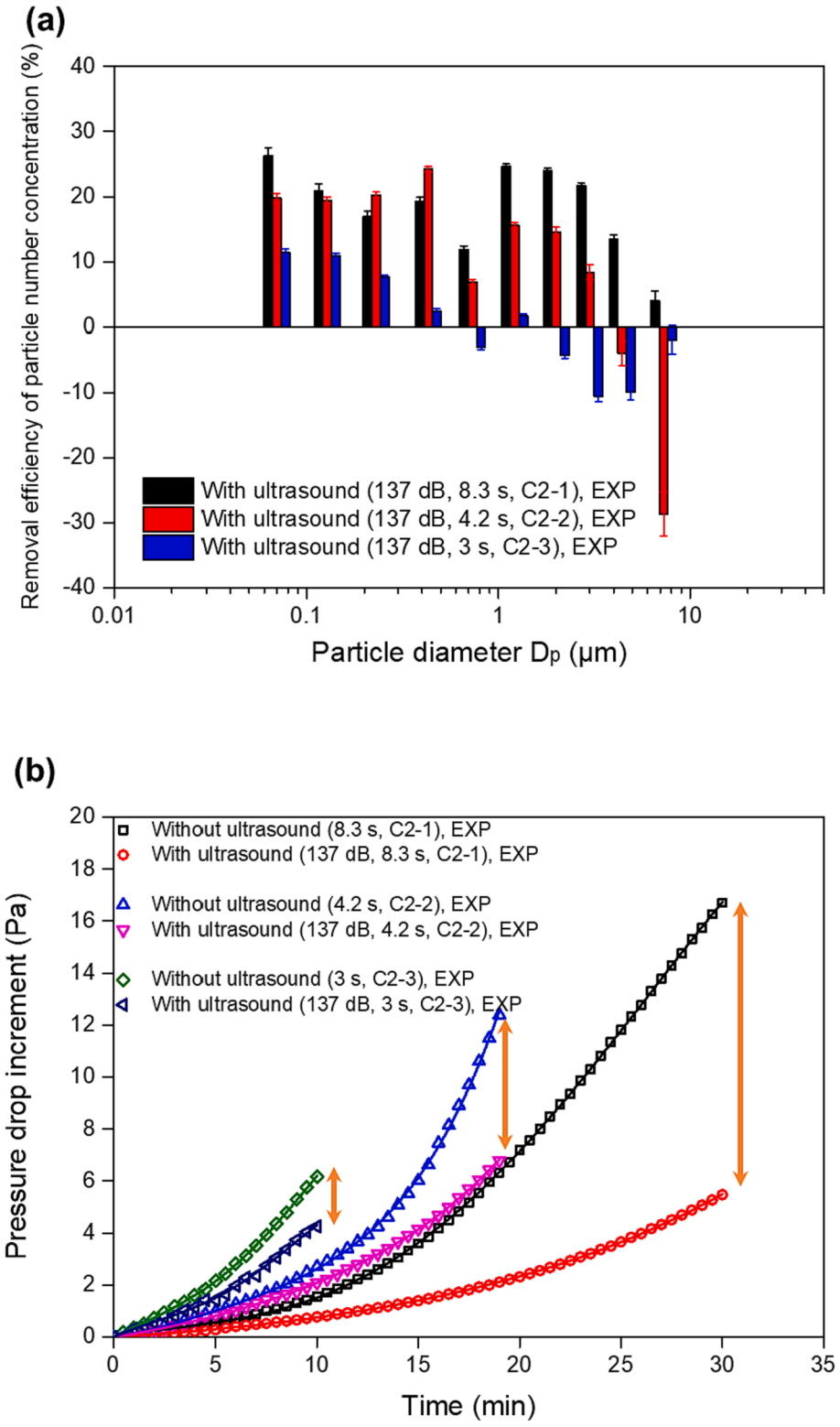

Fig. 4. Comparison of particle and filter characteristics without and with ultrasonication of 137 dB under different residence time. The initial total particle number concentrations are denoted as C2-1, C2-2, and C2-3, respectively. (a) Measured removal efficiency of particle number concentration versus particle diameter. (b) Measured time-domain pressure drop increment of air filters.

potentially experience a slower increase in PD. To validate this assumption, particles settled at the bottom of the cyclone without and with ultrasonication are collected to perform the scanning electron microscopy (SEM) characterization. As shown in Fig. 3(c), the particles that experience ultrasonication undergo agglomeration and are evidently larger as compared to those without ultrasonication. Furthermore, the comparison of the PSD spectra after the cyclone (before the air filter) shows that PNCs with ultrasonication also experience decrease across all the measurable particle size bins from 0.1 to 10 μm (Fig. 3(d)).

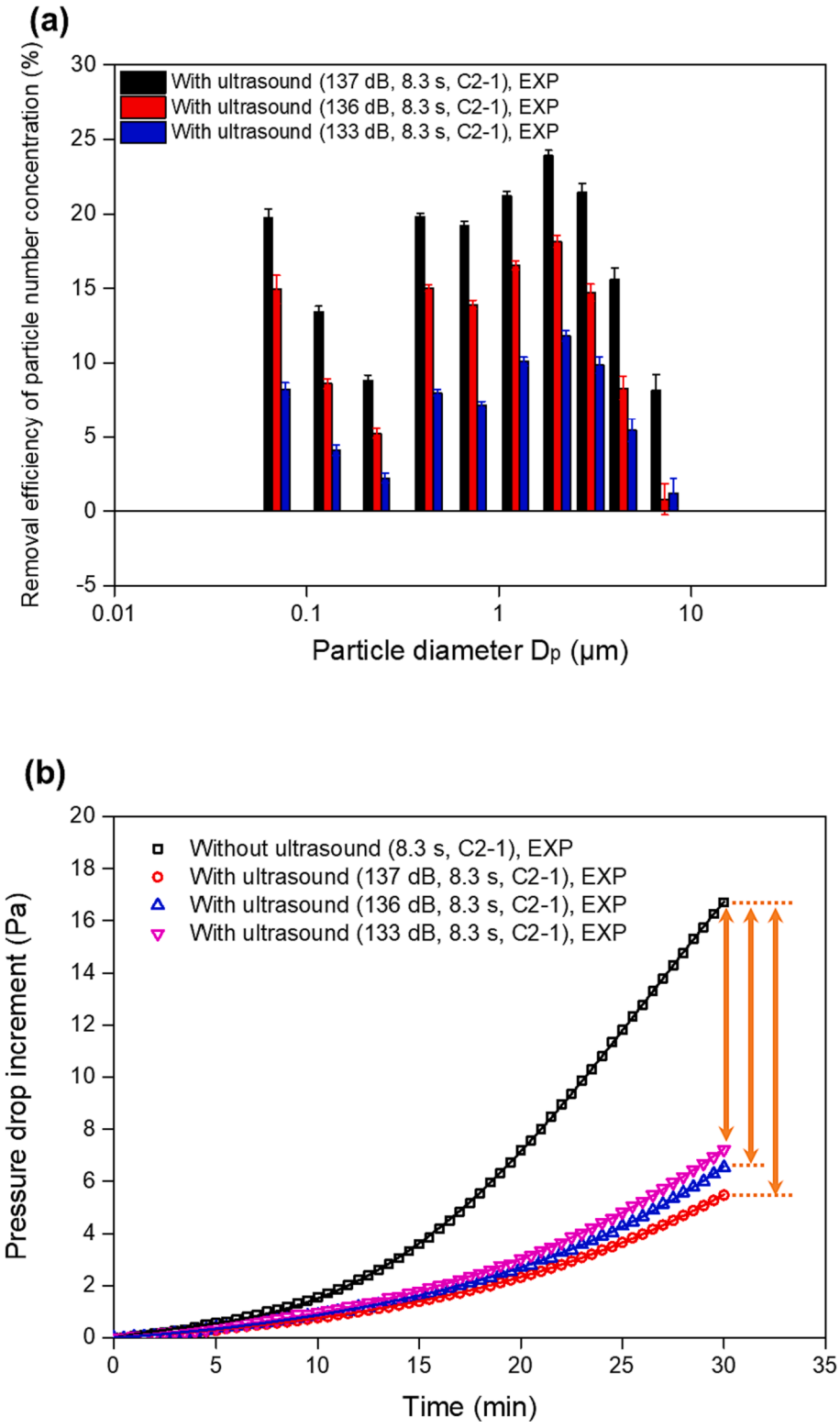

Fig. 5. Comparison of particle and filter characteristics without and with ultrasonication under the residence time of 8.3 s for different SPLs. The initial total particle number concentration is denoted as C2-1. (a) Measured removal efficiency of particle number concentration versus particle diameter. (b) Measured time-domain pressure drop increment of air filters.

Fig. 3(e) shows the measured time-domain PD increment across test filters without and with ultrasonication. Here, the PD increment is defined as its difference between its real-time and initial values. With ultrasonication, the PD increment across the filter rises less rapidly as compared to that without ultrasonication, and in the same duration of 30 min, the total PD increment of the filter with ultrasonication is reduced by around 20 % of that without ultrasonication. These results validate our design purpose of slowing down PD across air filters through the combination of the ultrasonic aerosol agglomeration and the cyclone-based particle deposition processes.

4.1. Effects of residence time

The effects of key acoustic and aerosol parameters on ultrasonic agglomeration and filter PD performances are experimentally investigated. Firstly, the experimental SPL and initial PNC released into the tunnel are kept constant, while the flow speed in the agglomeration zone is varied. This affects the residence time, which is the duration that aerosol particles are subjected to the maximum influence of ultrasonication. In order to keep the initial PNC constant under different flow speeds, the dispensing rate of the aerosol dispenser have to be increased as the flow speed increases. Here, the initial total PNCs are measured and denoted as C2-1, C2-2, and C2-3 under the combinations of the dispensing rate of 15 % and the flow speed of 0.36 m/s, the dispensing rate of 30 % and the flow speed of 0.72 m/s, and the dispensing rate of 70 % and the flow speed of 1 m/s, respectively (Table 2). The comparison of the initial PSDs under C2-1, C2-2, and C2-3 is given in Fig. S1 (Supplementary Material).

Fig. 4(a) shows the removal efficiency of PNC versus particle diameter under different residence time. As observed, increasing residence time can increase the removal efficiency of PNC for most particle size bins due to the longer duration of ultrasonic agglomeration process. Also, under the residence time of 3 s and 4.2 s, there is an increase in PNCs for larger particle size bins, which may result from the agglomeration of smaller particles into larger ones. Fig. 4(b) shows the measured time-domain PD increment of air filters without and with ultrasonication for different residence time. The increase in PD increment is more gradual with the increase in residence time as the higher agglomeration efficiency leads to the improved cyclone performance and hence less particle mass reaching the filters. Notably, for the residence time of 8.3 s, the total PD increment of the filter with ultrasonication of 30 min is reduced by 67.3 % of that without ultrasonication.

4.2. Effects of sound pressure level

The performance of ultrasonic aerosol agglomeration and the resultant PD increment across filters are also experimentally investigated under the experimental SPLs of 133 dB and 136 dB (under the transducer driving powers of 15 W and 30 W, respectively), respectively. Fig. 5(a) shows the removal efficiency of PNC versus particle diameter under different SPLs when the residence time and initial PNC are kept constant. It can be observed that a higher SPL enables higher removal efficiencies of PNC across all the particle size bins. Theoretically, this can be partially explained by the stronger influence of the orthokinetic and hydrodynamic effects under a higher SPL (Eqs. (4) and (7)). Similarly, for the time-domain PD increment across filters in Fig. 5(b), an increase in SPL leads to a slower increase in PD increment with reasons similar to the increase in residence time as explained earlier.

4.3. Effects of initial particle number concentration

To investigate the influence of initial PNC on ultrasonic aerosol agglomeration as well as PD increment across filters, the PNC released into the tunnel from the particle dispenser is varied. Apart from C1 and C2-2, a higher initial total PNC of C3 is considered, and it relies on the combination of the 100 % dispensing rate of the dust generator and the flow speed of 0.72 m/s in the agglomeration zone (Table 2). The comparison of the initial PSDs under C1, C2-2, and C3 is given in Fig. S1 (Supplementary Material). Fig. 6(a) shows the removal efficiency of PNC versus particle diameter under different initial total PNCs (C3 > C2-2 > C1) when the experimental SPL and residence time are kept constant. It is seen that overall, a higher initial PNC allows for higher removal efficiencies of PNCs. This is because with a higher initial PNC, particles are closer to each other at the beginning and thus more easily agglomerated under ultrasonication, thus resulting in better agglomeration effects. Fig. 6(b) shows the measured time-domain PD increment of air filters without and with ultrasonication for different initial total PNCs. It can be observed that the PD increment for C3 with ultrasonication, despite having the largest concentration, does not exhibit the expected largest difference in PD increment as compared to without ultrasonication. This is because during the experiments for C3, due to this high concentration, a single run of the dust generator with a fixed container with maximum contents can only sustain a short duration, thus making the corresponding time-domain PD increment data inconclusive. While comparing the PD increment results under C1 and C2-2 with ultrasonication, it can be seen that a higher initial PNC leads to a slower increase in PD increment as compared to its non-ultrasonication counterpart. This conclusion could also be extrapolated for C3 if the ultrasonication duration could be as long as that for C1 or C2-2.

4.4. Quantitative evaluation of pressure drop across filters

The effects of ultrasonication on the increase in PD increment across filters are evaluated in a more quantitative way through a defined performance factor. Firstly, the time taken for PD to reach twice the initial PD of air filter (meaning the PD increment is equal to the initial PD) without and with ultrasonication is denoted by τ_0 and τ, respectively. Next, a performance factor for PD is defined by $(\tau\text{-}\tau_0)/\tau_0 \times 100$ %. With this definition, Fig. 7(a) shows the relationship between the performance factor for PD against SPL when the residence time and initial total PNC are kept as 4.2 s and C2-2, respectively. It can be observed that increasing SPL improves the performance factor. Separately, when residence time is varied under a constant SPL of 137 dB across different initial total PNCs (Fig. 7(b)), it can be observed that the performance factor rises with the increase in residence time. It is worth mentioning that at some data points in Fig. 7, the performance factors are higher than 50 %, meaning that it would take more than 1.5 times of operation duration for an air filter to reach twice its initial PD with the ultrasonic aerosol agglomeration as compared to that without ultrasonication. This slower increase in PD across air filters could enable savings in energy consumption of exhaust fans in gas cleaning process lines in industrial plants [1,42], which is one of our future study directions.

5. Conclusion

In this study, the combined use of the ultrasonic aerosol agglomeration and a particle deposition technique is demonstrated to realize favorable changes in pressure drop across air filters in a purpose-built aerosol wind tunnel system. This is different from the conventional application of acoustic agglomeration which is mostly applied for aerosol emission control. The process is realized by the ultrasonic agglomeration of aerosol particles to transform small particles into larger agglomerates for the enhanced deposition in a subsequent particle separation device. Owing to this more efficient particle separation process, a downstream air filter receives less particle mass, resulting in a slower increase in its pressure drop as compared to the case without ultrasonic aerosol agglomeration. The agglomeration performance is evaluated through a series of numerical simulations and experimental investigations. Parametric studies are performed on the effects of residence time, sound pressure level, and initial particle number concentration on the ultrasonic aerosol agglomeration performance and PD

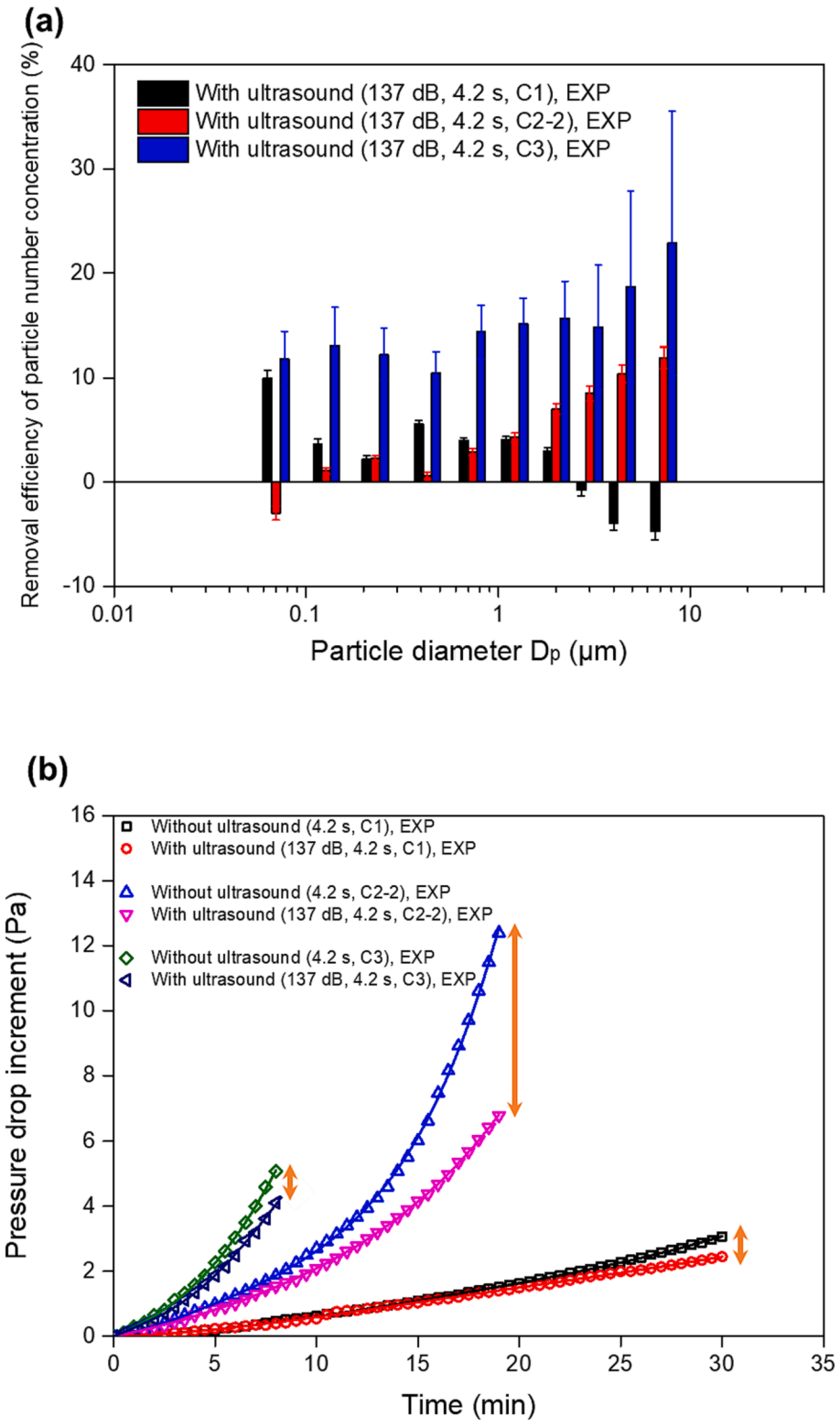

Fig. 6. Comparison of particle and filter characteristics without and with ultrasonication of 137 dB under the residence time of 4.2 s for different initial particle number concentrations. The initial total particle number concentration is varied between C3 > C2-2 > C1. (a) Measured removal efficiency of particle number concentration versus particle diameter. (b) Measured time-domain pressure drop increment of air filters.

increment across air filters. Our study indicates that besides application in aerosol emission control, the acoustic agglomeration technique is also capable of improving the operation characteristics of air filters (*i.e.*, pressure drop here) in a tunnel system. This is promising to not only prolonging service lives of air filters (by more than 50 % indicated in this study) but also enabling energy savings in exhaust fans (for overcoming air filter pressure drop) in industrial gas treatment processes and other ventilation systems.

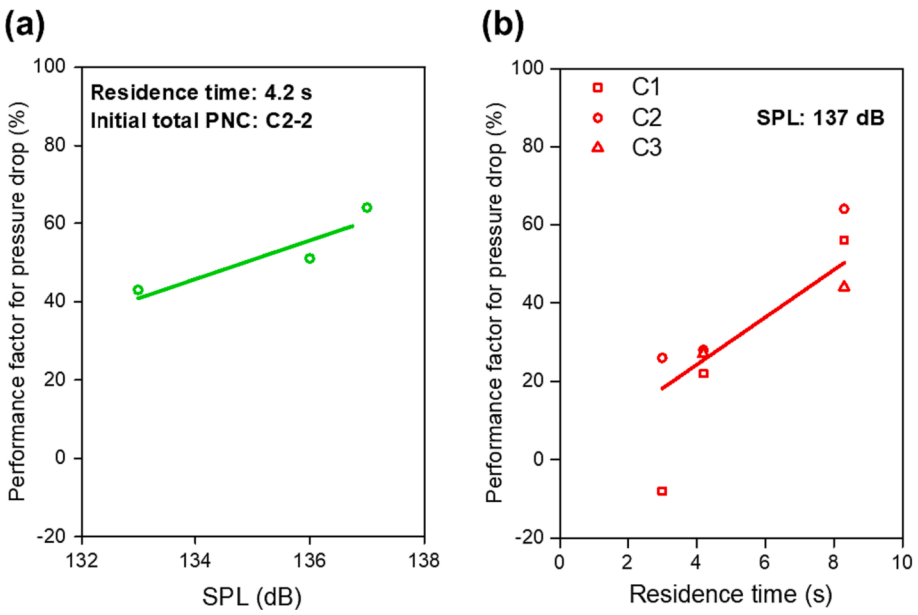

Fig. 7. (a) Performance factor for pressure drop versus SPL when the residence time and initial total particle number concentration are kept as 4.2 s and C2-2, respectively. (b) Performance factor for pressure drop versus residence time under different initial total particle number concentrations when the SPL is kept as 137 dB.

CRediT authorship contribution statement

Pengzhan Liu: Writing – original draft, Methodology, Investigation, Formal analysis, Data curation. **Xin Zhang:** Writing – review & editing, Methodology, Investigation, Formal analysis, Data curation. **Guicai Liu:** Writing – review & editing, Investigation. **Man Pun Wan:** Conceptualization, Methodology, Formal analysis, Supervision, Funding acquisition. **Grzegorz Lisak:** Writing – review & editing, Supervision, Funding acquisition. **Bing Feng Ng:** Conceptualization, Methodology, Formal analysis, Supervision, Funding acquisition, Writing – review & editing.

Declaration of competing interest

The authors declare that they have no known competing financial interests or personal relationships that could have appeared to influence the work reported in this paper.

Acknowledgments

This research is supported by the National Research Foundation, Singapore, and the Energy Market Authority, under its Energy Programme (EP Award EMA-EP009-SEGC-007). Any opinions, findings and conclusions or recommendations expressed in this material are those of the author(s) and do not reflect the views of National Research Foundation, Singapore and the Energy Market Authority. The authors would like to thank Dr. Shirun Ding for his advice in the experiments and Dr. Xiaopeng Shang for his advice in the simulations.

Appendix A. Supplementary data

Supplementary data to this article can be found online at https://doi.org/10.1016/j.ultsonch.2024.106774.

References

[1] B.F. Ng, J.W. Xiong, M.P. Wan, Application of acoustic agglomeration to enhance air filtration efficiency in air-conditioning and mechanical ventilation (ACMV) systems, PLoS One 12 (2017) e0178851.
[2] J. Ban, X. Wen, H. Xu, Z. Wang, X. Liu, G. Cao, G. Shao, J. Hu, Dual evolution in defect and morphology of single-atom dispersed carbon based oxygen electrocatalyst, Adv. Funct. Mater. 31 (2021) 2010472.
[3] P. Rao, D. Wu, T.J. Wang, J. Li, P. Deng, Q. Chen, Y. Shen, Y. Chen, X. Tian, Single atomic cobalt electrocatalyst for efficient oxygen reduction reaction, eScience 2 (2022) 399–404.
[4] J. Ban, H. Xu, G. Cao, Y. Fan, W.K. Pang, G. Shao, J. Hu, Synergistic effects of phase transition and electron-spin regulation on the electrocatalysis performance of ternary nitride, Adv. Funct. Mater. 33 (2023) 2300623.
[5] Y. Sun, S. Wang, D. Jiao, F. Li, S. Qiu, Z. Wang, Q. Cai, J. Zhao, C. Sun, Two-dimensional Pt2P3 monolayer: A promising bifunctional electrocatalyst with different active sites for hydrogen evolution and CO2 reduction, Chinese Chem Lett 33 (2022) 3987–3992.
[6] Y. Guo, J. Zhang, Y. Zhao, S. Wang, C. Jiang, C. Zheng, Chemical agglomeration of fine particles in coal combustion flue gas: Experimental evaluation, Fuel 203 (2017) 557–569.
[7] H. Bin, Y. Yang, Z. Lei, S. Ao, L. Cai, Y. Linjun, S. Roszak, Experimental and DFT studies of PM2.5 removal by chemical agglomeration, Fuel 212 (2018) 27–33.
[8] Y. Liu, B. Hu, L. Zhou, Y. Jiang, L. Yang, Improving the Removal of Fine Particles with an Electrostatic Precipitator by Chemical Agglomeration, Energy Fuel 30 (2016) 8441–8447.
[9] D. Chen, K. Wu, J. Mi, Experimental investigation of aerodynamic agglomeration of fine ash particles from a 330 MW PC-fired boiler, Fuel 165 (2016) 86–93.
[10] Z. Sun, L. Yang, S. Chen, L. Bai, X. Wu, Promoting the removal of fine particles and zero discharge of desulfurization wastewater by spray-turbulent agglomeration, Fuel 270 (2020).
[11] Z. Sun, L. Yang, H. Wu, X. Wu, Agglomeration and removal characteristics of fine particles from coal combustion under different turbulent flow fields, J. Environ. Sci. (China) 89 (2020) 113–124.
[12] M.D. Cheng, S.L. Allman, G.M. Ludtka, L.R. Avens, Collection of airborne particles by a high-gradient permanent magnetic method, J. Aerosol. Sci. 77 (2014) 1–9.
[13] J. Wang, W. Huang, H. Xu, H. Wang, Y. Ding, Z. Qu, N. Yan, Charged movement characteristics and enhanced removal of fine particles under the electric fields coupling with turbulence from industrial flue gas, Fuel 326 (2022).
[14] T. Mori, H. Nagashima, Y. Ito, Y. Era, J. Tsubaki, Agglomeration of fine particles in water upon application of DC electric field, Miner. Eng. 133 (2019) 119–126.
[15] H. Liu, Z. Li, H. Tan, F. Yang, P. Feng, Y. Du, M. Ren, M. Dong, Experimental investigation on a novel agglomeration device based on charged ultrasonic spray and vortex generators for improving the removal of fine particles, Fuel 287 (2021).
[16] R.F. Boucher, O.O. Okeke, High-gradient magnetic filtration of paramagnetic dust using woven wire matrix, Aerosol Sci. Tech. 12 (1990) 300–311.
[17] A.S. Mohammed, B.S. Yilbas, H. Al-Qahtani, A.A. Abubakar, M. Hawwa, M. Kassas, Dust mitigation from inclined hydrophobic and hydrophilic surfaces under electrostatic repulsion, J. Electrostat. 109 (2021) 103536.
[18] X. Xu, X. Gao, P. Yan, W. Zhu, C. Zheng, Y. Wang, Z. Luo, K. Cen, Particle migration and collection in a high-temperature electrostatic precipitator, Sep. Purif. Technol. 143 (2015) 184–191.
[19] O. Brandt, E. Hiedemann, The aggregation of suspended particles in gases by sonic and supersonic waves, Trans. Faraday Soc. 32 (1936) 1101–1110.
[20] J. Somers, J. Magill, K. Richter, S. Fourcaudot, P. Lajarge, P. Barraux, Acoustic agglomeration of liquid and solid aerosols: a comparison of a glycol fog and titanium dioxide, J. Aerosol. Sci. 22 (1991) S109–S112.
[21] Y. Ono, T. Asami, H. Miura, Agglomeration of aerosol using small equipment with two small aerial ultrasonic sources, Jpn. J. Appl. Phys. 62 (2023) SJ1029.

[22] L. Song, Modeling of acoustic agglomeration of fine aerosol particles, in: Department of Mechanical Engineering, 1990.
[23] K. Kilikeviciene, R. Kacianauskas, A. Kilikevicius, A. Maknickas, J. Matijosius, A. Rimkus, D. Vainorius, Experimental investigation of acoustic agglomeration of diesel engine exhaust particles using new created acoustic chamber, Powder Technol. 360 (2020) 421–429.
[24] J.A. Gallego-Juarez, E.R.F. De Sarabia, G. Rodriguez-Corral, T.L. Hoffmann, J. C. Galvez-Moraleda, J.J. Rodriguez-Maroto, F.J. Gomez-Moreno, A. Bahillo-Ruiz, M. Martin-Espigares, M. Acha, Application of acoustic agglomeration to reduce fine particle emissions from coal combustion plants, Environ. Sci. Tech. 33 (1999) 3843–3849.
[25] G.X. Zhang, L.L. Zhang, J. Wang, E. Hu, Improving acoustic agglomeration efficiency by addition of sprayed liquid droplets, Powder Technol. 317 (2017) 181–188.
[26] F. Fan, M. Zhang, Z. Peng, J. Chen, M. Su, B. Moghtaderi, E. Doroodchi, Direct simulation monte carlo method for acoustic agglomeration under standing wave condition, Aerosol. Air Qual. Res. 17 (2017) 1073–1083.
[27] P.Z. Liu, Z.H. Tian, N.J. Hao, H. Bachman, P.R. Zhang, J.H. Hu, T.J. Huang, Acoustofluidic multi-well plates for enrichment of micro/nano particles and cells, Lab Chip 20 (2020) 3399–3409.
[28] P. Liu, Z. Tian, K. Yang, T.D. Naquin, N. Hao, H. Huang, J. Chen, Q. Ma, H. Bachman, P. Zhang, X. Xu, J. Hu, T.J. Huang, Acoustofluidic black holes for multifunctional in-droplet particle manipulation, Sci. Adv. 8 (2022).
[29] P. Liu, H. Huang, X. Wang, Q. Tang, X. Qi, S. Su, Z. Xiang, J. Hu, Acoustic black hole profiles for high-performance ultrasonic tweezers, Mech. Syst. Signal Pr. 188 (2023) 109991.
[30] E. Riera, I. González-Gomez, G. Rodríguez, J.A. Gallego-Juárez, Ultrasonic agglomeration and preconditioning of aerosol particles for environmental and other applications, in: J.A. Gallego-Juárez, K.F. Graff (Eds.) Power Ultrasonics: Applications of High-Intensity Ultrasound, Woodhead Publishing, 2015, pp. 1023-1058.
[31] X.P. Shang, B.F. Ng, M.P. Wan, J.W. Xiong, S. Arikrishnan, Numerical investigation of spatially nonhomogeneous acoustic agglomeration using sectional algorithm, Aerosol. Sci. Tech. 52 (2018) 872–885.
[32] G. Shen, X. Huang, C. He, S. Zhang, L. An, Experimental study of acoustic agglomeration and fragmentation on coal-fired ash with different particle size distribution, Powder Technol. 325 (2018) 145–150.
[33] D. Zhou, Z.Y. Luo, J.P. Jiang, H. Chen, M.S. Lu, M.X. Fang, Experimental study on improving the efficiency of dust removers by using acoustic agglomeration as pretreatment, Powder Technol. 289 (2016) 52–59.
[34] L. Wu, G. Zhang, Y. Huihui, Z. Ma, Z. Chi, S. Liu, Study on agglomeration of ultrafine droplet particles by acoustic air-jet generators, IOP Conf. Ser.: Mater. Sci. Eng. 721 (2020) 012026.
[35] J.P. Yan, L.Q. Chen, Z. Li, Removal of fine particles from coal combustion in the combined effect of acoustic agglomeration and seed droplets with wetting agent, Fuel 165 (2016) 316–323.
[36] K. Zu, Y. Yao, M. Cai, F. Zhao, D.L. Cheng, Modeling and experimental study on acoustic agglomeration for dust particle removal, J. Aerosol. Sci. 114 (2017) 62–76.
[37] Z.Y. Luo, H. Chen, T. Wang, D. Zhou, M.S. Lu, M.C. He, M.X. Fang, K.F. Cen, Agglomeration and capture of fine particles in the coupling effect of pulsed corona discharge and acoustic wave enhanced by spray droplets, Powder Technol. 312 (2017) 21–28.
[38] Y. Yang, Q. Cao, Y. Wang, H. Chen, Y. Zhang, M. Qiao, Y. Zhou, N. Zhu, Agglomeration of oil droplets assisted by low-frequency sonic pretreatment, Powder Technol. 428 (2023) 118860.
[39] Y. Guo, G. Zhang, Y. Li, H. Gu, D. Yuan, M. Liu, Study on aerosol agglomeration using the airborne ultrasonic transducer, Particuology 82 (2023) 157–165.
[40] Y. Hoda, T. Asami, H. Miura, Aerosol agglomeration by aerial ultrasonic sources containing a cylindrical vibrating plate with the same diameter as a circular tube, Jpn. J. Appl. Phys. 61 (2022) SG1073.
[41] Y.T. Zhang, S.K. Lai, J.C.W. Yu, H. Guo, C.W. Lim, A novel U-shaped acoustic-manipulated design to enhance the performance of low-efficiency filters for sub-micron particles, Powder Technol. 392 (2021) 412–423.
[42] D. Ma, Q. Zheng, W. Lin, M. Guo, Improvements to dust filtration through acoustic agglomeration and atomization, Aerosol Sci. Tech. 51 (2017) 824–832.
[43] S.K. Friedlander, Smoke, Dust, and Haze: Fundamentals of Aerosol Dynamics, 2nd ed., Oxford University Press, 2000.
[44] E.P. Mednikov, Acoustic Coagulation and Precipitation of Aerosols, Springer, New York, 1965.
[45] C. Sheng, X. Shen, Modelling of acoustic agglomeration processes using the direct simulation Monte Carlo method, J. Aerosol. Sci. 37 (2006) 16–36.
[46] L. Song, G.H. Koopmann, T.L. Hoffmann, An improved theoretical model of acoustic agglomeration, J. Vib. Acoust. Trans. ASME 116 (1994) 208–214.
[47] F. Gelbard, Y. Tambour, J.H. Seinfeld, Sectional representations for simulating aerosol dynamics, J. Colloid Interf. Sci. 76 (1980) 541–556.
[48] F. Gelbard, J.H. Seinfeld, Simulation of multicomponent aerosol dynamics, J. Colloid Interf. Sci. 78 (1980) 485–501.
[49] O.A. Ezekoye, Y.W. Wibowo, Simulation of acoustic agglomeration processes using a sectional algorithm, J. Aerosol. Sci. 30 (1999) 1117–1138.